Physical Chemistry Chemical Physics

PCCP

Phase diagrams of nanoalloys: influence of size and morphology.

Journal:	*Physical Chemistry Chemical Physics*
Manuscript ID:	CP-ART-03-2015-001593.R1
Article Type:	Paper
Date Submitted by the Author:	06-May-2015

Complete List of Authors:	Berthier, Fabienne; CNRS, Univ. Paris Sud, ICMMO/SP2M Maras, Emile; Univ. Paris Sud, ICMMO/SP2M Legrand, Bernard; CEA, DEN, SRMP

Journal Name

RSCPublishing

ARTICLE

Phase diagrams of nanoalloys: influence of size and morphology.

Cite this: DOI: 10.1039/x0xx00000x

F. Berthier[a,b], E. Maras[b,c] and B. Legrand[d]

Received 00th January 2012,
Accepted 00th January 2012

DOI: 10.1039/x0xx00000x

www.rsc.org/

The size dependence of the phase diagram of nanoalloys with a tendency to phase separation is investigated. As the critical temperature may depend on both the size and the morphology of the nanoparticles, we consider nanowires with different cross-sections and also nanotubes with different circumferences. The variation of the critical temperature with the length of all these nanoparticles is systematically studied using Monte Carlo simulations based on an Ising model. A non-monotonic variation of the critical temperature is observed as a function of the length. The maximal value of the critical temperature is reached when the length and the circumference of the nanoparticles are similar. The phase diagrams obtained within two thermodynamic ensembles (the canonical ensemble and the pseudo grand canonical ensemble) are compared and discussed in terms of the behaviour of a single particle or an assembly of nanoparticles in mutual equilibrium with each other.

1. Introduction

Nano-objects with shape as different as nanowires[1-5], nanotubes[6,7] or truly three-dimensional[8-10] (3D) nanoparticles, can now be obtained experimentally. When they are built with two types of atoms (A and B), the knowledge of their phase diagram is a very topical issue[11-14]. For instance, the magnetic properties of CoPt nanoalloy are observed only in the $L1_0$ ordered state and disappear above the critical temperature T_c, *i.e.,* in the disordered state.[15] In this system, it has been shown experimentally that T_c is much lower than the size of the nanoparticle is small.[15] Moreover, for a given size of the nanoparticle, the aspect ratio also affects the critical temperature.[15]

The purpose of this paper is to study the influence of the size and the shape of nanoalloys on their phase diagram, and more specifically on the critical temperature. To simplify the study, we consider a very simple Ising model to investigate a generic binary system A_cB_{1-c} with a tendency to phase separation, *i.e.* with a miscibility gap at low temperature in the bulk phase diagram. For such a system, we have previously shown that the critical temperature for a finite one-dimensional (1D) chain is not zero[16], whereas it is well-known that T_c for an infinite chain is equal to zero.[17] That means that, contrary to the results mentioned above for the 3D Co-Pt nanoalloys[14], the critical temperature increases for the 1D chain when its length decreases.[16]

To determine how the variation of T_c depends on the dimensionality of the nanoparticles, we investigate nanoalloys with different shapes, allowing one to study the change when going progressively from the 1D case to the 2D case. Thus, for a given length, we consider nanowires with cross-sections going from 1 to 4 sites and also hollow nanotubes with different circumferences. We will see that varying the aspect ratio by changing the circumference (or the cross-section) for a given length or by changing the length for a given circumference allows one to observe a change between 1D-type and 2D-type behaviour.

To determine the phase diagram and the variation of the critical temperature with the size and the shape of the nanoparticles, we perform Monte Carlo simulations both in the canonical ensemble and in the pseudo grand canonical (PGC) ensemble. In the canonical ensemble the nominal concentration is fixed, reproducing the case of an isolated nanoparticle. In the PGC ensemble, the alloy chemical potential is imposed and this can be viewed as an assembly of nanoparticles in equilibrium with each other. If it is well-known that both ensembles lead to the same phase diagram for infinite systems[18], this result is not guaranteed for finite system.[14,19-21] For instance, it may depend on the choice of the concentration (nominal concentration or core concentration) used to define the phase diagram of the nanoparticle.

The paper is organized as follows: Section 2 presents the description of the various clusters studied (§ 2.1) and gives some details on the energetic model and the formulas allowing the connection between the canonical and the PGC ensembles (§ 2.2). In Section 3, we detail the behaviour at high temperature (§ 3.1) and low temperature (§ 3.2) for the four-chain nanowire, *i.e.*, the nanowire with a cross-section of four sites, before presenting the phase diagram for all the nanoparticles studied (§ 3.3). Section 4 is devoted to the analysis of the size and the shape effects on the critical temperature. Finally, we outline the main results in the conclusion.

2. Model

2.1. Nanowires and nanotubes

To go progressively from the 1D geometry to the 2D case, we consider nanowires constituted by a single chain (NW-1C, fig. 1a), two chains (NW-2C, fig. 1b) and four chains (NW-4C, fig. 1c). We also consider nanotubes having a section (or a circumference) equals to $n_s = 8$ atoms (NT-8C, fig. 1d) and $n_s = 12$ atoms (NT-12C, fig. 1e). For each particle, all the sites have the same coordination number Z, except the sites at the extremities which have one bond less than the common sites. Their coordination number is then: $Z_e = Z - 1$ (see Table 1).

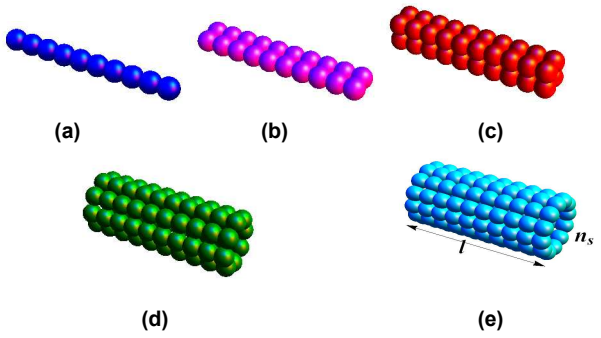

Fig. 1 Nanowires and nanotubes considered in the present study. l denotes the length and n_s the section of the nanoparticles. Nanowires constituted by a single chain (NW-1C, $n_s = 1$) (a), two chains (NW-2C, $n_s = 2$) (b), four chains (NW-4C, $n_s = 4$) (c), and nanotubes with $n_s = 8$ atoms (NT-8C) (d) and $n_s = 12$ atoms (NT-12C) (e), illustrated for a length $l = 10$ atoms.

If the single chain is a pure 1D object, the nanotubes can be viewed as 2D objects, in the sense that they are equivalent to planes with a finite direction along the length of the nanotubes and a periodic boundary condition (with the size of the box equal to the circumference) in a perpendicular direction. The NW-2C is the first step to go from the 1D object to the 2D objects, whereas the NW-4C is the more close-packed object with an isotropic 3D character for the 8 sites cube ($l = 2$) followed by a 2D or almost 1D character when the length becomes much larger than the circumference.

Table 1 summarizes the structural characteristics of the different nano-objects.

Table 1 Structural characteristics of the different nanowires and nanotubes considered here: size of the section (expressed as a number of sites) (n_s), coordination number for the common sites (Z) and for the extremity sites (Z_e).

	nanowires			nanotubes	
n_s	1	2	4	8	12
Z	2	3	4	4	4
Z_e	1	2	3	3	3

2.2. Ising model and Monte Carlo simulations

We consider an Ising model[22] which is governed by only two parameters when considering core and extremity properties for A_cB_{1-c} nanoalloys (or bulk and surface properties for semi-infinite alloys): $\tau = (V^{AA} - V^{BB})/2$ and $V = (V^{AA} + V^{BB} - 2V^{AB})/2$, where V^{AA}, V^{BB} and V^{AB} are the nearest-neighbour pair interactions between $A-A$, $B-B$ and $A-B$ atoms respectively. For the sake of consistency with previous studies, we kept the same set of energetic parameters which describes the main features of Ag_cCu_{1-c} system: $\tau = 46$ meV and $V = -30$ meV[13,23-26]. The positive value of τ, which reproduces the lower cohesive energy of Ag as regards to Cu (in absolute value), leads to the Ag segregation for the less coordinated sites.[27,28] The negative value of V reproduces the tendency to phase separation in Cu-Ag alloys and leads to the existence of a critical temperature for infinite 3D and 2D alloys[22]. In the mean-field approximation, the critical temperature T_c is proportional to the coordination number according to the relation: $k_BT_c = Z|V|/2$. However, the mean field approximation overestimates the exact critical temperatures by a factor which depends on the crystallographic structure.[29] Actually, this factor depends on both the coordination number and the dimensionality. Figure 2 shows the exact critical temperature as a function of the coordination number for 1D, 2D and 3D infinite systems and illustrates the difference between the mean-field approximation and the exact calculations.[29] For example, for a coordination number equal to 6, the exact value of T_c for the 2D triangular lattice is lower than the value for the 3D simple cubic lattice, itself lower than the value obtained within the mean-field approximation (see figure 2).

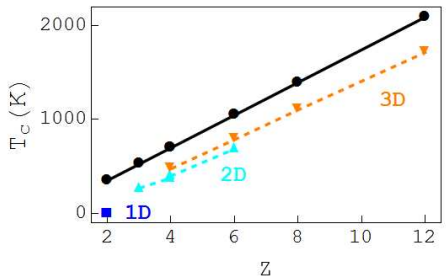

Fig. 2 Critical temperature for $V = -30$ meV as a function of the coordination number. Exact value for 1D system (in blue square), 2D systems: honeycomb ($Z = 3$), square ($Z = 4$) and triangular ($Z = 6$) lattices (in cyan up-triangles), 3D systems: diamond ($Z = 4$), simple cubic ($Z = 6$), bcc ($Z = 8$) and fcc ($Z = 12$) lattices (in orange down-triangles) and within the mean-field approximation (black circles).

To analyze how the critical temperature vary for finite objects, the phase diagrams for the different nanoparticles described above are determined by means of Monte Carlo simulations, both in the canonical and in the PGC ensembles. Actually, for finite systems, the different thermodynamic ensembles are not equivalent[18-20] and a careful study in each ensemble is required to determine the size dependence of the critical temperature for nanoparticles.

For infinite or semi-infinite systems, an efficient way to determine the phase diagram is to calculate the isotherm $\Delta\mu(c)$ or $c(\Delta\mu)$, where $\Delta\mu = \mu_{Ag} - \mu_{Cu}$ is the alloy chemical potential and c is the Ag concentration. $c = n_{Ag}/n$, where n_{Ag} is the number of Ag atoms and n is the total number of sites ($n = n_s\, l$). In the canonical ensemble, the nominal concentration c is fixed by the relative proportion of Ag and Cu atoms initially introduced in the nanoparticle. Then $\Delta\mu$ is calculated using the Widom method[30] to obtain the isotherm $\Delta\mu(c)$. Note that the elementary event proposed in the Widom method is a transmutation from Cu to Ag in the different sites of the nano-objects and not an insertion of an atom as in the original work of Widom[30]. For the transmutation event on a rigid lattice, the convergence is very fast, contrary to what can be observed for the insertion events[31]. In the PGC ensemble, $\Delta\mu$ is imposed and the nominal concentration may fluctuate around its equilibrium value fixed by the value of $\Delta\mu$. In this case, the isotherm $c(\Delta\mu)$ is obtained.

Note that the PGC quantities can be deduced from the canonical simulations too. For a given value of $\Delta\mu^P$ (the exposant P indicates that this is a PGC quantity), the nominal concentration c^P is the PGC thermodynamic average of all the possible concentrations:

$$c^P(\Delta\mu^P) = \sum_{n_A=0}^{n_A=n} \frac{n_A}{n} P_{n_A}^P(\Delta\mu^P), \quad (1)$$

where $P_{n_A}^P(\Delta\mu^P)$, the probability that the nanoparticle contains n_A atoms A, is defined by:

$$P_{n_A}^P(\Delta\mu^P) = \frac{Z_{n_A}^P(\Delta\mu^P)}{Z^P(\Delta\mu^P)}. \quad (2)$$

$Z^P(\Delta\mu^P)$ is the PGC partition function and $Z_{n_A}^P(\Delta\mu^P)$ is the partition function of the system constrained to have the composition $c = n_A/n$. $Z^P(\Delta\mu^P)$ is given by:

$$Z^P(\Delta\mu^P) = \sum_{n_A=0}^{n_A=n} Z_{n_A}^P(\Delta\mu^P), \quad (3)$$

and $Z_{n_A}^P(\Delta\mu^P)$ is expressed as a function of the canonical partition function Z_{n_A} at the same composition n_A:

$$Z_{n_A}^P(\Delta\mu^P) = Z_{n_A} exp(n_A \Delta\mu^P / k_B T). \quad (4)$$

The canonical partition function Z_{n_A} can be deduced from the canonical isotherm $\Delta\mu(n_A)$ following:

$$Z_{n_A} = Z_{n_A-1} exp(-\Delta\mu(n_A)/k_B T), \quad (5)$$

with $Z_{n_A=0} = 1$ and $Z_{n_A=n} = exp(-2N_b\tau/k_B T)$, where N_b is the total number of bonds in the nanoparticle.

Eqs. (1-5) provide the link between the PGC ensemble and the canonical one. They show that for a given value of $\Delta\mu^P$ the PGC ensemble is a weighted average of canonical sub-ensembles of different compositions. Eqs. (1-5) will be used to compare the solubility limits in both ensembles. In practice the application of these formulae to get PGC isotherms requires determining the canonical isotherm for $n_A \in]0, n[$ with a good accuracy. We have verified that the comparison between PGC Monte Carlo simulations and calculations based on Canonical Monte Carlo simulations and Eqs. (1-5) lead to a perfect agreement.

3. Isotherm and phase diagram

As previously mentioned, the determination of the phase diagrams requires calculating the isotherms at different temperatures. We focus on the nanowire constituted by four chains (NW-4C, fig. 1c) of length l = 10 to illustrate the methodology described in the previous section.

3.1. High temperature

At high temperature (800 K), the isotherms $\Delta\mu(c)$ obtained from MC simulations are monotonous. Furthermore, they are rather similar in both ensembles (fig. 3a). In the PGC ensemble, the fluctuations of the nominal concentration around the mean value are characterized by means of the concentration density of states (CDOS) $P_c^P(\Delta\mu)$ (fig. 3b). $P_c^P(\Delta\mu)$ gives the probability that the nanoparticle has a concentration c for a given value of the alloy chemical potential. At high temperature and for a finite object, the concentration distribution has one maximum and is close to a gaussian distribution (fig. 3b). Ag and Cu atoms are located almost randomly in the nanowire whatever the thermodynamic ensemble considered. This is illustrated by the snapshot shown in figure 3c. A more detailed characterization shows a slight Ag enrichment at the extremities due to the less cohesive energy of Ag, as mentioned previously[23-26,28].

3.2. Low temperature

At low temperature (400 K) the canonical isotherm is no more monotonic. A decreasing part occurs in the Ag-rich region (fig. 4a). This indicates that two states have the same free energy, the equal areas rule allowing one to define the concentrations c_α and c_β and the critical value $\Delta\mu_c$ (see fig. 4b) by the equation:

$$\int_{c_\alpha}^{c_\beta} (\Delta\mu - \Delta\mu_c)\, dc = 0. \quad (6)$$

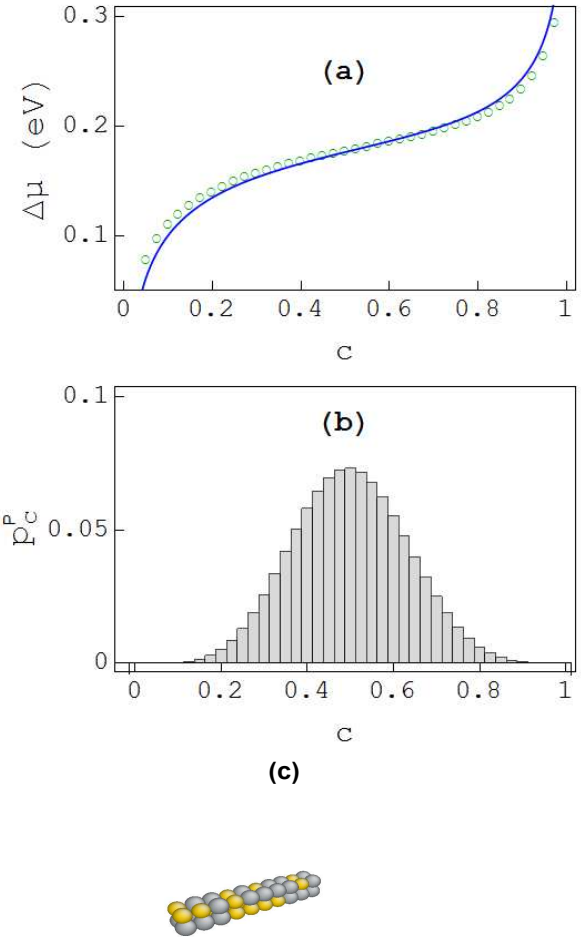

Fig. 3 Isotherms $\Delta\mu(c)$ at $T = 800$ K obtained from Monte Carlo simulations in the canonical ensemble (green circles) and in the PGC ensemble (blue line) for the NW-4C (a). Concentration density of states for the PGC ensemble at $\Delta\mu = 177$ meV (corresponding to $c \approx 0.5$) (b). Snapshot at $c = 0.5$ (c). Cu atoms are in yellow and Ag atoms are in grey. The NW-4C nanowire consists of four chains of length $l = 10$.

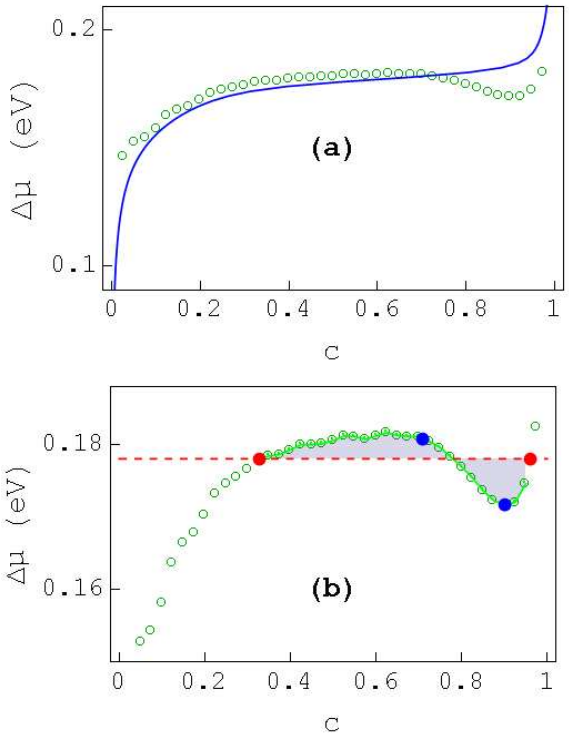

Fig. 4 Isotherms $\Delta\mu(c)$ at $T = 400$ K obtained from Monte Carlo simulations in the canonical ensemble (green circles) and in the PGC ensemble (blue line) for the NW-4C building with four chains of length $l = 10$ (a). Figure (b) is an enlargement of the canonical isotherm shown in (a). The horizontal dashed line (in red) indicates the critical value of $\Delta\mu$. The areas (in grey) situated on either side of the horizontal line are equal. Red points indicate the solubility limits c_α and c_β, and blue points the limits of the phase-separated regime $\tilde{c}_\alpha$ and $\tilde{c}_\beta$.

For an infinite alloy, these concentrations correspond to the solubility limits of the alloy. Between these two limits, the stable configuration of the infinite alloy is a phase-separated state with the spatial coexistence of two states of concentration c_α and c_β. For a **single** nanoparticle, the spatial coexistence of two states is not possible since each state incorporates all the sites of the nanoparticle including the extremities. Therefore, the concentrations c_α and c_β do not correspond to any observable change of the configuration for an isolated particle.

At the opposite, the extrema of the canonical isotherm concentration $\tilde{c}_\alpha$ and $\tilde{c}_\beta$ correspond to the limits of the phase-separated regime (see fig. 4b). In this regime, the Ag-riche phase is located near the extremities and the Cu-rich phase is in the core of the nanoparticle. The concentration $\tilde{c}_\alpha$ separates the single phase regime with Ag segregation at the extremities from the phase separation regime with the Ag-rich phase starting from the extremities. Similarly, $\tilde{c}_\beta$ separates the single Ag-rich phase regime from the phase separation regime with the minority Cu-rich phase in the core (fig. 5).

The extremum corresponding to $\tilde{c}_\beta$ is much more pronounced than the one corresponding to $\tilde{c}_\alpha$. At $\tilde{c}_\beta = 0.9$, the first Cu nucleus occurs in the Ag-rich nanowire, forming one plate of four Cu atoms in the core (referred to as a plate of one monolayer thickness hereafter), see fig. 5b. Conversely, for the Cu-rich nanowire, Ag segregation at the extremities initiates a wetting phenomenon, which extends up to $\tilde{c}_\alpha$. This corresponds to the continuous increase of the thickness of the Ag-rich region from the extremities towards the core as the concentration increases. $\tilde{c}_\alpha$ $(= 0.7)$ corresponds to the end of this regime, when the Cu-rich region is reduced to a plate of three monolayers thickness (12 Cu atoms), with two interface layers and one core layer (fig. 5a).

Thus, even if the range where the canonical isotherm $\Delta\mu(c)$ is a decreasing function allows one to define unambiguously the concentrations $\tilde{c}_\alpha$ and $\tilde{c}_\beta$, the meaning of these two quantities differ from one another. $\tilde{c}_\beta$ separates clearly the single phase from the two-phase regime in the Ag-rich nanowire, whereas $\tilde{c}_\alpha$ indicates the end of the wetting regime. Due to the occurrence of the wetting in the Cu-rich nanowires, the distinction between the single phase regime (with Ag segregation at the extremities) and the phase separation regime cannot be easily done for *isolated* nanowires, *i.e.* in the canonical ensemble.

(a) (b)

Fig. 5 Snapshot of the NW-4C nanowire of length $l = 10$ at $c = \tilde{c}_\alpha$ (a) and $c = \tilde{c}_\beta$ (b) in the canonical ensemble at $T = 400$ K. Cu atoms are in yellow and Ag atoms are in grey.

Contrary to the high temperature case, the PGC isotherm differs substantially from the canonical one at low temperature (fig. 4a). In particular, a decreasing part is not observed in the PGC isotherm, which is a monotonic function as at high temperature. However, the CDOS strongly differs from the high temperature case: a bimodality is observed in a narrow range of $\Delta\mu$ centered around $\Delta\mu_c$ (fig. 6). In this range of $\Delta\mu$, the nanoparticle oscillates during a PGC-simulation between two states, one being Cu-rich, the other being almost pure in Ag. A physical realisation of the PGC ensemble is to consider an assembly of nanoparticles in mutual equilibrium. In this case, the bimodality of the CDOS may be interpreted as the coexistence of Cu-rich and Ag-rich nanowires in the assembly of nanoparticles.

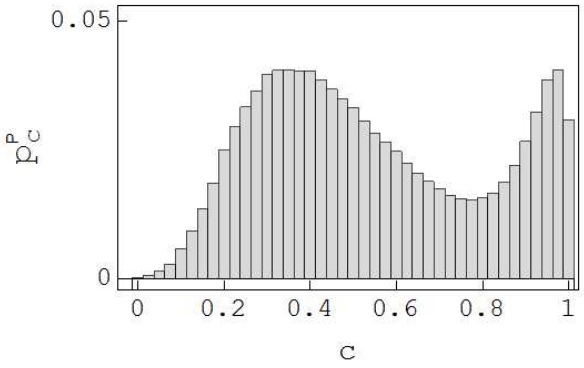

Fig. 6 Concentration density of states for the NW-4C nanowire of length $l = 10$ in the PGC ensemble at $\Delta\mu_c = 178$ meV and $T = 400$ K.

When increasing $\Delta\mu$ in the range of the CDOS bimodality, the probability to observe the Ag-rich phase increases and the one to observe the Cu-rich phase one decreases (fig. 7a). This evolution is continuous and explains the monotonic increase of c in the PGC isotherm, contrary to the non-monotonic behaviour of the canonical isotherm.

Fig. 7a also shows that the concentration corresponding to the Ag-rich peak is almost independent of $\Delta\mu$, whereas the concentration of the Cu-rich mode increases with $\Delta\mu$. A similar phenomenon is also observed for semi-infinite alloys in the vicinity of the solubility limit. This is a consequence of the wetting phenomenon[23]. The thickness of the Ag-rich wetting layer formed at each extremity of the Cu-rich nanowire increases with $\Delta\mu$, leading to an increase of the concentration of the Cu-rich state.

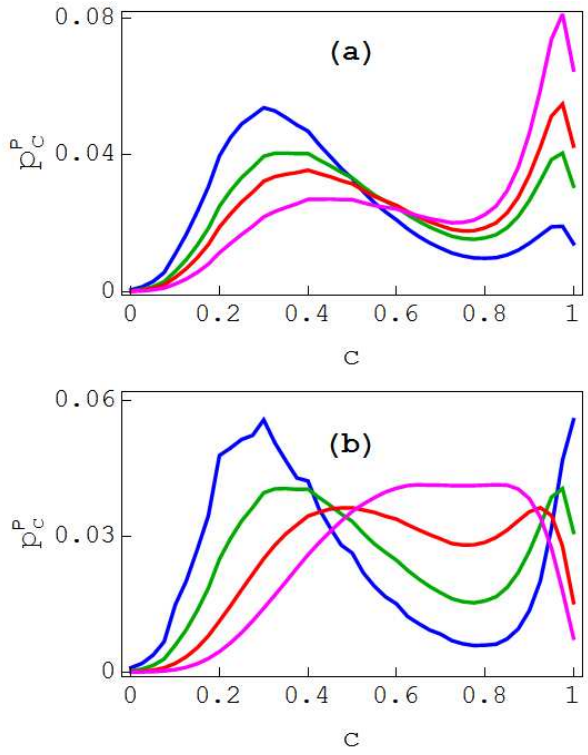

Fig. 7 Evolution of the CDOS as a function of $\Delta\mu$ at T = 400 K (a) and as a function of T for $\Delta\mu = \Delta\mu_c$ (b) for the NW-4C nanowire of length $l = 10$. Only the contours of the histograms are drawn. In (a) $\Delta\mu$ = 177 meV: blue, 178 meV: green, 179 meV: red and 180 meV: magenta. In (b) $T = 350$ K ($\Delta\mu_c = 177$ meV): blue, $T = 400$ K ($\Delta\mu_c = 178$ meV): green, $T = 450$ K ($\Delta\mu_c = 180$ meV): red and $T = 500$ K ($\Delta\mu_c = 182$ meV): magenta.

Looking now at the evolution of the critical CDOS (*i.e.,* for $\Delta\mu = \Delta\mu_c(T)$) as a function of the temperature (fig. 7b), we observe that the concentration of the Ag-rich peak varies very slightly with the temperature. On the contrary, the concentration of the Cu-rich peak increases significantly with T. This implies that the concentration corresponding to the top of the miscibility gap is expected to be shifted towards the high concentration side.

The isotherms being different in both thermodynamic ensembles, one can wonder if this is also the case for the so-called "solubility limits" c_α and c_β defined previously in the canonical ensemble, see Eq. 6. Using the multiple segment trapezoidal rule, Eq. 6 may be written as:

$$(1/n)k_B T \ln\left(Z_{c_\alpha}/Z_{c_\beta}\right) - (c_\beta - c_\alpha)\Delta\mu_c = 0. \quad (7)$$

Using Eqs. (3-4), the above expression leads to the equality:

$$P^P_{c_\alpha}(\Delta\mu_c) = P^P_{c_\beta}(\Delta\mu_c). \quad (8)$$

Eq. (8) demonstrates that in the PGC ensemble and for $\Delta\mu = \Delta\mu_c$ the configurations corresponding to $c = c_\alpha$ and $c = c_\beta$ have the same probability of occurrence. It is also possible to show that c_α and c_β correspond to maxima of the CDOS. It

means that both ensembles are consistent and lead to the same phase diagram if this one is defined by the curves $c_\alpha(T)$ and $c_\beta(T)$, in analogy with the phase diagram of infinite alloys.

However, if experiments are performed on an isolated nanoparticle, the extrema of the canonical isotherm concentration $\tilde{c}_\alpha$ and $\tilde{c}_\beta$ are more useful than c_α and c_β to characterize the phase separation regime. For an assembly of nanoparticles, *i.e.*, in the PGC ensemble, c_α and c_β are a good indication of the mean concentration of the two populations occurring in the vicinity of $\Delta\mu_c$. However, the knowledge of all the CDOS is important; in particular, the relative areas of the two peaks give the proportion of the two populations in coexistence. Moreover, the fact that the position of the low-concentration peak, *i.e.*, the Cu-rich state, shifts as a function of $\Delta\mu$ (being equal to c_α only for $\Delta\mu = \Delta\mu_c$), reinforces the interest of knowing the whole CDOS and not just c_α and c_β.

3.3. Phase diagram

Up to now, we considered the nominal concentration of the nanoparticles, without distinguishing the concentration of the extremities from the concentration of all the other sites. In order to compare the phase diagram of the nanoparticles with the one of the infinite alloy, it is better to get ride of the obvious effect of segregation and wetting at the extremities which will have all the more importance as the nanowire is short. To this aim, we draw the phase diagram of the nanoalloys as a function of the concentration of the sites located in the central section of the nanoparticles (hereafter referred to as the core concentration c_{core}) and not of the nominal concentration. In this representation of the phase diagram, we plot the core concentrations corresponding to the nominal concentrations c_α and c_β determined by Eq. (6) in the canonical ensemble.

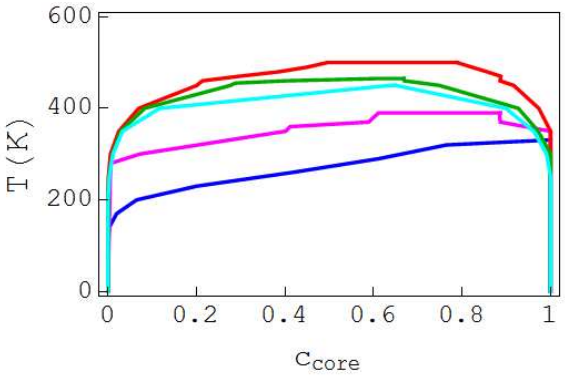

Fig. 8 Phase diagrams of nanowires and nanotubes of length $l = 10$. The colour convention is the same as in fig. 1: nanowires constituted by a single chain (blue), two chains (magenta), four chains (red), and nanotubes with a circumference of $n_s = 8$ sites (green) and $n_s = 12$ sites (cyan).

Figure 8 shows the resulting phase diagrams of all the nanoparticles (nanowires and nanotubes) of length $l = 10$. Considering the core concentration does not suppress the asymmetry of the phase diagram of the nanoparticles, whereas the bulk phase diagram is obviously symmetric due to the symmetry of the Ising model. The asymmetry is very pronounced for the single chain and decreases when increasing the circumference (fig. 8). Moreover, the asymmetry occurs only in a limited range of temperature, *i.e.*, for temperature higher than about 0.6 T_c, where T_c is the critical temperature of the nanoparticle. This is related to the fact that the concentration profile starting from the extremities is less damped when T increases[23].

Fig. 8 indicates that the phase diagram of the finite linear chain exhibits a large miscibility gap, whereas it is well-known that the critical temperature of an infinite 1D system is nil[17]. More generally, by comparing figs. 8 and 2, we observe that the critical temperature of all structures of length l = 10 is higher than the critical temperature of the infinite equivalent systems. Moreover, T_c increases with the coordination number Z, but is not at all proportional to Z contrary to infinite systems.

4. Critical temperature

The critical temperature for nanowires and nanotubes with length l = 10 being higher than for infinite equivalent systems, it is tempting to conclude that T_c decreases when the size of the nanoparticle increases. However, experimental results on 3D nanoparticles in CoPt system conclude the opposite result: T_c increases with the system's size!

To elucidate this paradox, we systematically calculated the critical temperature for the various nanowires and nanotubes as a function of their length. In the canonical ensemble, T_c is determined as the temperature for which the decreasing part of the isotherm disappears to give way to a plateau at $\Delta\mu = \Delta\mu_c$ for a large range of concentration. In the PGC ensemble, T_c is defined as the temperature for which the bimodal CDOS becomes monomodal for $\Delta\mu = \Delta\mu_c$. However, due to the large plateau observed in the CDOS in the vicinity of T_c (see fig. 7b), the accurate determination of the critical temperature is not easy in the PGC ensemble and the canonical ensemble is more appropriate for this.

Fig. 9 depicts the variation of T_c as a function of the length l for the nanowires and the nanotubes. The critical temperature is a decreasing function of the length for the nanowires constituted by one chain and two chains. For the single chain, this result is in perfect agreement with the asymptotic behaviour of T_c for large l: $T_c^{1D} \approx 2|V|/k_B lnl$ obtained from the analytical derivation of the canonical partition function[16], see fig. 9.

Contrary to the nanowires with one or two chains, the nanowire constituted by four chains and the nanotubes present a variation of T_c, which is not monotonic as function of l. T_c goes through a maximum for value of l close to the circumference n_s. For $l < n_s$ the critical temperature increases with the size, as expected for 2D and 3D objects[15]. For $l > n_s$, T_c decreases when l increases, recovering the behaviour observed for the 1D (single chain) or the almost 1D (two chains) systems.

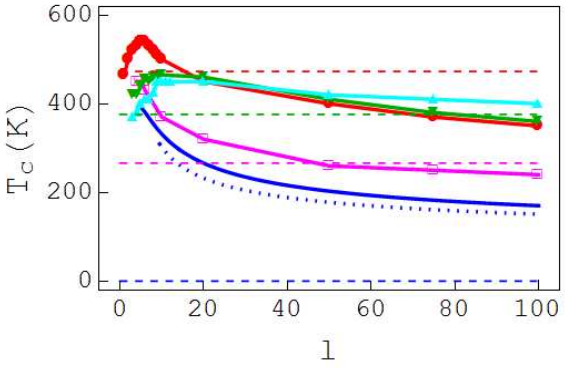

Fig. 9 Evolution of the critical temperature as a function of the length of the nanowires and nanotubes. The colour convention is the same as in fig. 1: nanowires constituted by a single chain (blue), two chains (magenta), four chains (red), and nanotubes with a circumference of $n_s = 8$ sites (green) and $n_s = 12$ sites (cyan). For comparison, the critical temperature of different infinite systems (with dimensionality D and coordination Z) are indicated in dashed lines: $D = 1, Z = 2$ (linear chain) in blue, $D = 2, Z = 3$ (honeycomb) in magenta, $D = 2, Z = 4$ (square) in green and $D = 3, Z = 4$ (diamond) in red. The dotted blue curve denotes the asymptotic behaviour of the linear chain.

Thus, the origin of the paradoxal variation of T_c with the size of the nanoparticle is cleared: for 1D or almost 1D systems (*i.e.*, when one dimension, the length, is much larger than the others), the critical temperature is a decreasing function of the length. At the opposite, for 2D and 3D systems, T_c is an increasing function of the length, consistently with the experimental observations on 3D CoPt nanoalloys[15].

5. Conclusions

Even by using a very simple energetic model, we have shown that the phase diagrams of nanoalloys are much more complex than their bulk counterpart. In particular, the physical interpretation of the solubility limits depends on the considered thermodynamic ensemble. This means that experiments performed on an isolated particle (reproduced by the canonical ensemble) or on an assembly of particles in mutual equilibrium (reproduced by the PGC ensemble) do not explore the same characteristics of the phase diagram. In the case of an assembly of nanoparticles, the knowledge of the whole CDOS is necessary to quantify the relative proportion of the particles rich in one element or the other at the vicinity of the critical alloy chemical potential.

Surface segregation (or segregation at the extremities for the nanowires and nanotubes) leads to a wetting phenomenon, which makes difficult to distinguish the single-phase state from the two-phase state for an isolated nanoparticle. Moreover, for $T > 0.6\, T_c$, the segregation profile induces an asymmetry of the phase diagram, even if we consider the core concentration and not the nominal concentration to avoid the trivial effect of the extremities enrichment on the nominal concentration.

Another important conclusion of this work is the influence of the nanoparticle morphology on the variation of the critical temperature with its size. If the system has one dimension (the "length") much larger than the others, it can be considered as almost 1D and T_c decreases with the length. At the opposite, when the nanoparticle is really 2D or 3D, T_c increases with its size. This result allows one to reconcile the increase of T_c with the size experimentally observed for 3D nanoparticles and the decrease of T_c for the linear chain as a function of the length, T_c vanishing for an infinite chain.

This work has to be considered only as a preliminary work on the influence of the size and the morphology on the phase diagrams of nanoalloys. Actually some additional factors are susceptible to modify these phase diagrams, such as the flexibility of nanoparticles or the relaxation and the possible reconstruction of the different facets of their outer shell[32]. Moreover, it is well-known that the value of the interactions may vary between the bulk and the surface sites[33,34]. Even their sign may change[35]. An extension to take into account all these factors to obtain the variation of the phase diagram with the size and the morphology of the nanoparticles is in progress.

Acknowledgements

It is a great pleasure to thank A. Ziani, J. Creuze, C. Mottet and G. Tréglia for very fruitful discussions.

Notes and references

[a] CNRS, UMR 8182, F91405 Orsay Cedex, France.
[b] SP2M/ICMMO, Univ. Paris Sud, F91405 Orsay Cedex, France.
[c] Department of Applied Physics and COMP CoE, Aalto University School of Science.
[d] CEA, DEN, Service de Recherches de Métallurgie Physique, F91191 Gif-sur-Yvette Cedex, France.

1 H. Fu, X. Yang, X. Jiang and A. Yu, *Langmuir*, 2013, **29**, 7134.
2 X. Hong, D. Wang, R. Yu, H. Yan, Y. Sun, L. He, Z. Niu, Q. Peng and Y. Li, *Chem. Commun*, 2011, **47**, 5160.
3 P. Thaler, A. Volk, F. Lackner, J. Steurer, D. Knez, W. Grogger, F. Hofer and W. E. Ernst, *Phys. Rev. B*, 2014, **90**, 155442.
4 C. Zhu, S. Guo and S. Dong, *Adv. Mater.*, 2012, **24**, 2326.
5 L. Wei, W. Qi, B. Huang and M. Wang, *Comput. Mat. Sci.*, 2013, **69**, 374.
6 E. M. Zahran, D. Bhattacharyya and L. G. Bachas, *J. Mater. Chem.*, 2011, **21**, 10454.
7 M. Mohl, D. Dobo, A. Kukovecz, Z. Konya, K. Kordas, J. Wei, R. Vajtai and P. Ajayan, *J. Phys. Chem. C*, 2011, **115**, 9403.
8 C. Langlois, D. Alloyeau, Y. Le Bouar, A. Loiseau, T. Oikawa, C. Mottet and C. Ricolleau, *Faraday Discuss*., 2008, **138**, 375.
9 C. Langlois, Z.L. Li, J. Yuan, D. Alloyeau, J. Nelayah, D. Bochicchio, R. Ferrando and C. Ricolleau, *Nanoscale*, 2012, **4**, 3381.
10 P. Andreazza, C. Mottet, C. Andreazza-Vignolle, J. Penuelas, H. C. N. Tolentino, M. De Santis, R. Felici and N. Bouet, *Phys. Rev. B*, 2010, **82**, 155453.
11 A.S. Shirinyan and M. Wautelet, *Nanotechnology*, 2004, **15**, 1720.
12 J. Pohl, C. Stahl and K. Albe, *Beilstein J. Nanotechnol.*, 2012, **3**, 1.

13 J. Creuze, F. Berthier and B. Legrand, *Nanoalloys: synthesis, structure and properties,* chap. 6, Springer-Verlag, London, 2012.
14 F. Calvo, *Phys. Chem. Chem. Phys.*, 2015, DOI :10.139/c5cp00274e
15 D. Alloyeau, C. Ricolleau, C. Mottet, T. Oikawa, C. Langlois, Y. Le Bouar, N. Braidy and A. Loiseau, *Nature Mater.*, 2009, **8**, 940.
16 E. Maras, Thesis, Univ. Paris Sud, Orsay, 2012.
17 H. E. Stanley, *Introduction to Phase Transitions and Critical Phenomena*, Clarendon Press, Oxford, 1971.
18 L. Van Hove, *Physica*, 1949, **15**, 951.
19 F. Gulminelli, *Ann. Phys. Fr.*, 2004, **29**, 1.
20 P. Chomaz, V. Duflot and F. Gulminelli, *Phys. Rev. Lett.*, 2000, **85**, 3587.
21 P. Labastie and R.L. Whetten, *Phys. Rev. Lett.*, 1990, **65**, 1567.
22 F. Ducastelle, *Order and Phase Stability in Alloys,* North-Holland, Amsterdam, 1991.
23 F. Lequien, Thesis, Univ. Paris Sud, Orsay, 2008.
24 F. Lequien, J. Creuze, F. Berthier and B. Legrand, *J. Chem. Phys*., 2006, **125**, 094707.
25 F. Lequien, J. Creuze, F. Berthier and B. Legrand, *Faraday Discuss*., 2008, **138**, 105.
26 F. Lequien, J. Creuze, F. Berthier, I. Braems and B. Legrand, *Phys. Rev. B*, 2008, **78**, 075414.
27 G. Tréglia, B. Legrand and F. Ducastelle, *Europhys. Lett*., 1988, **7**, 575.
28 F. Berthier, B. Legrand and G. Tréglia, *Acta Mater*., 1999, **47**, 2705.
29 M.E. Fisher, *Rep. Prog. Phys.*, 1967, **30**, 615.
30 B. Widom, *J. Chem. Phys.*, 1963, **39**, 2808.
31 M. Athènes, *Phys. Rev. E*, 2002, **66**, 046705.
32 M. Briki, J. Creuze, F. Berthier and B. Legrand, *Solid State Phenom.*, 2011, **172-174**, 658.
33 I. Braems, J. Creuze, F. Berthier, R. Tétot and B. Legrand, *Surf. Sci.,* 2008*,* **602**, 1903.
34 M. Polak and L. Rubinovich, *Phys. Rev. B*, 2009, **80**, 045404.
35 M. Briki, Thesis, Univ. Paris Sud, Orsay, 2013.

